Investigating the Al-Cr-La ternary system: Al-rich corner phase equilibria at 600 °C

Tilen Balaško[1], Adam Zaky[1], Simona Delsante[2]

[1]Faculty of Natural Sciences and Engineering, University of Ljubljana, Aškerčeva cesta 12, 1000 Ljubljana, Slovenia

[2]Department of Chemistry and Industrial Chemistry, Genoa University, Via Dodecaneso 31, Genoa I-16146, Italy

E-mail: tilen.balasko@ntf.uni-lj.si, adam.zaky@ntf.uni-lj.si, simona.delsante@unige.it

(Received 15 January 2026; Accepted 21 May 2026)

Abstract

The phase equilibria of the ternary phase system Al-Cr-La were investigated in the Al-rich corner at 600 °C, with minimum Al content of 98.77 at.%. The formed phases, transformation temperatures (specifically liquidus and solidus) and microstructure evolution were experimentally determined by isothermal annealing at 600 °C for 600 hours and Differential Scanning Calorimetry (DSC) analysis. Scanning Electron Microscope (SEM) equipped with Energy-Dispersive X-ray Spectroscopy (EDXS) was employed to completely characterize the samples. The equilibrium microstructure state consists of the (Al), the binary phase $Al_{45}Cr_7$ and the ternary phase $LaCr_2Al_{20}$ in the samples with increased Cr content (from 0.03 up to 1.12 at.%), while it consists of the (Al), the mixture (Al) + $Al_{11}La_3$ and the ternary $LaCr_2Al_{20}$ phase in the samples with increased La content (from 0.03 up to 0.45 at.%). It was observed that even the small amount of alloying elements leads to the formation of ternary phase.

Key words: Al-Cr-La, ternary phase system, phase equilibria, microstructure

1 Introduction

Aluminium alloys exhibit exceptional physical and mechanical properties, including high strength, good wear resistance, corrosion resistance, stiffness and elongation [1–6] This unique combination makes them a widely used structural material [7–9] in various transport industries, such as automotive [10–16], rail [17] and aerospace [18–20], mainly due to their high strength-to-weight ratio. In the EU, transport is responsible for 20% of all greenhouse gas (GHG) emissions, with road transport alone contributing 72% [21–23]. In fact, transport has the largest impact on GHG emissions of all sectors, including agriculture, industry, trade, and electricity generation [24,25]. More specifically, car transport contributes approximately 12% of total GHG emissions in the EU. Consequently, car manufacturers are obliged to reduce the average carbon emissions of their fleets by 37.5% between 2021 and 2030 [26]. A very effective strategy to achieve these reductions is to reduce vehicle weight, as lighter vehicles consume less fuel and therefore leave a smaller CO_2 footprint [23,27,28]. For this reason, as already mentioned aluminium alloys are already extensively utilized in the transport industry, and their application will continue to increase.

In order to improve the mechanical properties and suitability of aluminium alloys for the transport industry, they are often alloyed with rare earth elements (REE). In particular, the addition of La has been shown to refine the secondary dendrite arm spacing (SDAS) of the primary α-Al phase/grains [29–32]. Furthermore, previous studies [29–37] have consistently demonstrated that La additions improve both mechanical properties and corrosion resistance. In our previous work [38], we investigated the influence of La additions on a high-strength 7xxx Al-Zn-Mg-Cu alloy. This alloy typically contains small amounts of Cr. Surprisingly; La was found to form a ternary phase $LaCr_2Al_{20}$. This was unexpected as the CALPHAD calculations with Thermo-Calc [39], database TCAL9 (Al-Alloys v9.1) [40], did not show the phase and the ternary phase system Al-Cr-La is not included in the mentioned database and it is generally known that Cr and La do not normally form intermetallic phases with each other; this is explained in more detail in the literature review. The absence of this specific phase in the existing calculated ternary systems has motivated our current research on the Al-Cr-La ternary system. This ternary phase could be important for the development of the next generation of high-strength aluminium alloys of the 7xxx group, as it may potentially prevent excessive growth of the aluminium grain size. This would be beneficial in conjunction with the improvement of mechanical properties. As Cr has been added to most of these alloys, alloying with La leads to the formation of the ternary phase [38]. One of the objectives was to determine the minimum La and/or Cr content in the Al-rich corner at 600 °C to form a ternary phase $LaCr_2Al_{20}$ and also to study the evolution of the microstructure and phases present in the alloys.

In order to provide a better understanding of the phase equilibria in the ternary system Al-Cr-La, the three relevant binary phase diagrams described in the literature — Al-Cr, Al-La, and La-Cr — are briefly presented and the corresponding references are given. Limited experimental results for this ternary system are reviewed and the crystallographic information on its stable solid phases is presented in Table 3.

1.1 Binary systems

Al-Cr binary system

The binary Al-Cr phase diagram was analysed by Murray [41], relying largely on experimental data from Köster et al. [42]. This phase system is widely recognized and has been studied in detail by numerous researchers over the years [43–56], with the most recent study being conducted by S. Cui et al. [57]. The phases present in this binary system, and their corresponding crystal structures are listed in Table 1.

Table 1. Al-Cr crystal structure data

Phase	Composition at.% Cr	Space group	Pearson symbol	Prototype	Reference
(Al)	0-0.37	$Fm\bar{3}m$	$cF4$	Cu	[43]
Al_7Cr	12.5-1	$C2/m$	$mS104$	$Al_{45}V_7$	[41,43,57,58]
$Al_{11}Cr_2$	15.2-17	$P2$	$mP48$	-	[41,43,47,54,57]
Al_4Cr	18.5-20	$P2/m$	$mP180$	μ_Al_4Mn	[43,56,57]
$Al_{11}Cr_4$	25	$P\bar{1}$	$aP30$	-	[43,48]
αAl_9Cr_4	30-42	$I\bar{4}3m$	$cI52$	-	[41,43]
βAl_8Cr_5	30-42	-	-	-	[41,43]

αAl_8Cr_5	30-42	$R\bar{3}m$	$hR26$	Al_8Cr_5	[41,43]
AlCr	60.5-63	$Pm\bar{3}m$	$cP2$	CsCl	[43,55]
$AlCr_2$	65.5-71.4	$I4/mmm$	$tI6$	$MoSi_2$	[41,43,57]
(Cr)	54.5-100	$Im\bar{3}m$	$cI2$	W	[43]

Al-La binary system

The binary Al-La phase diagram was analysed by Gschneidner [59] mainly on the basis of Buschow's [60] investigation of the Al-La system. This binary system is also widely recognized and has been studied in detail by numerous researchers [61–72], with the most recent thermodynamic evaluation and optimization carried out by Jin et al. [65]. The phases present in this binary system and their corresponding crystal structures are listed in Table 2.

Table 2. Al-La crystal structure data

Phase	Composition at.% La	Space group	Pearson symbol	Prototype	Reference
$\alpha Al_{11}La_3$	0.01-21.4	$Immm$	$oI28$	$\alpha Al_{11}La_3$	[59,65,66,72]
$\beta Al_{11}La_3$	0.01-21.4	$I4/mmm$	$tI10$	Al_4Ba	[59,65,66,72]
Al_3La	21.4-25	$P6_3/mmc$	$hP8$	Ni_3Sn	[59,60,65,66,72]
Al_xLa or $La_{22}Al_{53}$	25-29.3	$P6_3/mmm$	$hP3$	AlB_2	[59,65,66]
Al_2La	29.3-33.3	$Fd\bar{3}m$	$cF24$	Cu_2Mg	[59,60,65,66,72]
AlLa	33.3-50	$Cmc2\ or\ Cmcm$	$oS16$	AlCe	[59,60,65,66,72]
$AlLa_3$	50-75	$P6_3/mmc$	$hP8$	Ni_3Sn	[59,60,65,66,72]
(γLa)	75-100	$Im\bar{3}m$	$cI2$	W	[59,65,72]
(βLa)	75-100	$Fm\bar{3}m$	$cF4$	Cu	[59,65,72]
(αLa)	75-100	$P6_3/mmc$	$hP4$	αLa	[59,65,72]

La-Cr binary system

The binary La-Cr phase diagram was redrawn by Massalski et al. [73] on the basis of the investigations by Barabash et al. [74]. This system has been studied less frequently compared to the two previously mentioned, although there are some studies [74–78]. The recent work by Chan et al. [78] was also included in the review by Okamoto [79]. As noted by Okamoto [79], there is a significant discrepancy regarding the maximum solubility of La in Cr. While earlier studies [75] suggested higher values, more recent work [76] indicates a much lower solubility of approximately 0.6 at.%. It is known that this system contains Cr, γLa, βLa and αLa phases. Since no binary intermetallic phases are formed in the La-Cr system, the crystal structure data for these constituent phases have already been presented in Table 1 and Table 2.

1.2 Al-Cr-La ternary phase diagram

The Al-Cr-La ternary system was first investigated by Kripyakevich et al. [80], who reported the existence of the ternary compound $LaCr_2Al_{20}$. Its existence and crystal structure were subsequently confirmed by Emes-Misenko [81] using X-ray diffraction (XRD) analysis. Emes-Misenko [81] identified three ternary phases (summarised in Table 3) and constructed the isothermal section at 500°C (Figure 1); however, the precise composition ranges for these phases remain largely undetermined.

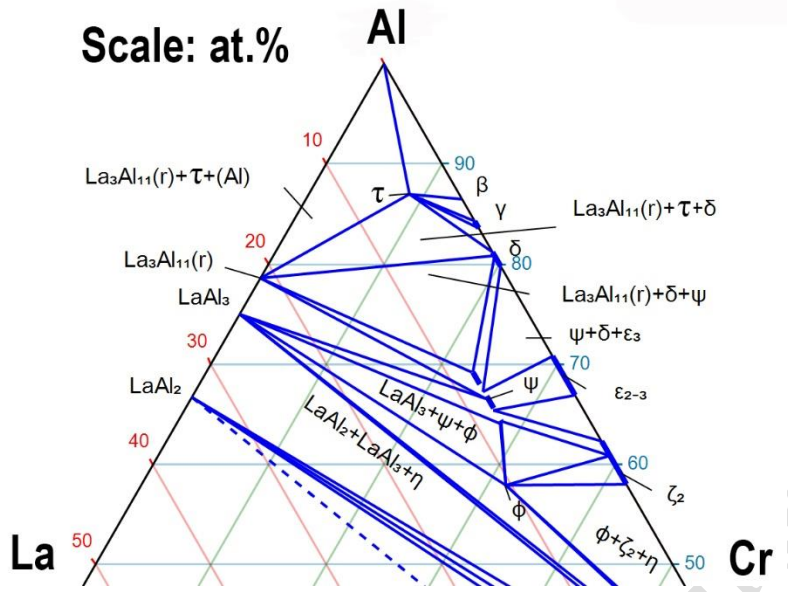

Figure 1. Partial isothermal section through the ternary phase diagram of Al-Cr-La at 500 °C [82]

Table 3. Al-Cr-La crystal structure data

Phase	Pearson symbol	Prototype	Reference
$LaCr_2Al_{20}$ or τ	$cF184$	$Mg_3Cr_2Al_{18}$	~4.5La-9Cr-86.5Al [81,82]
$LaCr_{4-x}Al_{8+x}$ or ψ Or $LaCr_4Al_8$ Or $LaCr_3Al_9$	$tI26$	$ThMn_{12}$	not a homogeneity range, but two different compositions reported: x = 0 [82,83] x = 1 [81,82]
$La_2Cr_6Al_{11}$ or φ	$hR19$	Th_2Zn_{17}	[81,82]

In the Al-rich corner, $LaCr_2Al_{20}$ is known to exist; however, specific data on its minimum and maximum Cr and La content are still lacking in the literature. The 1971 study [81] remains the only comprehensive investigation of the phase equilibria in this system. Although more recent studies [84, 85] have examined $LnCr_2Al_{20}$ compounds (Ln = La, Gd, Yb), their primary focus was the interaction of conduction electrons with local magnetic moments. These works are relevant as they confirm the structural stability of the $LnCr_2Al_{20}$-type phases, but they do not provide the thermodynamic or compositional data required for industrial alloy design.

2 Experimental methods

2.1 Sample preparation

Pure aluminium (99.99 wt.%, WAV AG "Kryal"), chromium (99.99 wt.%, Thermo Scientific Chemicals) and lanthanum (99.99 wt.%, JM Alfa Aesar) were used as starting materials for the alloy production. The alloys, each weighing 3 g, were produced as button-shaped castings with approximate dimensions of 20 mm in diameter and 5–10 mm in thickness. These were

fabricated in a vacuum arc melting system (MTI SP-MSM208) using a non-consumable tungsten electrode on a water-cooled copper hearth. A high purity argon atmosphere (Ar 6.0, 99.999%) was maintained, which was further purified by melting a titanium getter (99.7 wt.%). The protective gas pressure in the furnace was 50 kPa at room temperature. Before the introduction of argon, the melting chamber was evacuated, and the residual pressure was monitored with a vacuum gauge. The alloys were remelted four times to ensure chemical homogeneity. Prior to annealing, the chemical composition of the samples was checked using a Thermo Fisher Scientific Quanta 650 scanning electron microscope (SEM) equipped with an Oxford Instruments AZtec Live, Ultim Max SDD 40 mm^2 system for energy-dispersive X-ray spectroscopy (EDXS). An accelerating voltage of 20 kV was used for all SEM/EDXS analyses to ensure accurate quantification and appropriate penetration depth. Homogenization was carried out in a Xiamen Tmax Battery Equipments Limited SK2-4-12TPB3 tube furnace under an inert argon (Ar 5.0, 99.999%) atmosphere. Before the protective gas was introduced, the tube was evacuated four times with a vacuum pump, and the residual pressure was continuously monitored with a vacuum gauge. To further purify the inert gas and prevent oxidation, magnesium crisps (99.99 wt.%) were added to the tube to act as an oxygen carrier. The samples were placed on the Al_2O_3 crucibles before homogenization, which was carried out at 600 °C for 600 hours. After the homogenization process, the samples were quenched in ice-cold water to maintain the equilibrium structure.

2.2 Differential scanning calorimetry (DSC)

The phase transformation temperatures were determined with a SETARAM Labsys EVO device equipped with a DSC rod. The DSC was calibrated with high purity standards of In (99.99%), Sn (99.99%), Al (99.99%) and Ag (99.99%) from the NETZSCH standard calibration set. A high-purity argon atmosphere (Ar, 99.9999%) was used as a protective gas. Prior to sample analysis, a baseline correction run was performed at a heating/cooling rate of 5 °C/min, ranging from 25°C to 1100 °C and back to 25 °C. All samples were then analysed using the temperature program mentioned above. Al_2O_3 crucibles with a lid were used for all runs, including calibration, correction, and sample analysis. To ensure accuracy in identifying the melting sequences, DSC heating curves were evaluated by determining the characteristic onset and peak temperatures. These were interpreted using the methodologies established by Boettinger et al. [86] for complex multicomponent systems, in which the sequence of endothermic events corresponds to the successive dissolution of phases until the liquidus is reached.

2.3 Microstructure analysis

The samples for microstructural analysis were ground on silicon carbide paper and then polished with a diamond-water suspension on cloth discs. Prior to SEM-EDXS (Energy-Dispersive X-ray Spectroscopy) analysis, all metallographic samples underwent quality control of the polished surface using a Leica DM4000 M optical microscope equipped with the AxioCam ERc 5s high-resolution digital camera. The microstructure was then analysed using the Zeiss EVO 40 SEM with PentaFET EDXS detector (Oxford Instruments). The BSE (Backscattered Electron) mode was used to capture the images.

3 Results and Discussion

In order to analyse the aluminium-rich corner in the Al-Cr-La ternary phase diagram, 10 alloys with higher Cr (1-5) and La (6-10) content were produced. The global chemical composition is shown in Table 4 (compositions are calculated averages measured with EDXS); in addition to the chemical composition, the same table also lists the corresponding equilibrium phases at 600 °C for each alloy produced. The results show that a ternary $LaCr_2Al_{20}$ phase forms , even with the addition of La and/or Cr at concentrations as low as 0.03 at.%. The phases were determined by SEM-EDXS. As the ideal stoichiometry of the $LaCr_2Al_{20}$ phase is established in the literature, EDXS analysis was performed to confirm the presence of this phase and to determine its actual composition in the investigated samples. It should be noted that the $Al_{11}La_3$ phase (Table 4) is in the eutectic mixture with Al, this will be further discussed during the metallographic and DSC analysis. As the phases were only analysed by EDXS, the phase assignments are estimates based on the chemical composition obtained.

Table 4. Chemical composition of the samples with the corresponding equilibrium phases in the microstructure

Sample	at.%			Detected phases		
	Al	Cr	La			
1	98.89	1.08	0.03	$Al_{45}Cr_7$	$LaCr_2Al_{20}$	(Al)
2	98.83	1.12	0.05	$Al_{45}Cr_7$	$LaCr_2Al_{20}$	(Al)
3	99.08	0.84	0.08	$Al_{45}Cr_7$	$LaCr_2Al_{20}$	(Al)
4	98.92	0.95	0.13	$Al_{45}Cr_7$	$LaCr_2Al_{20}$	(Al)
5	98.77	1.00	0.23	$Al_{45}Cr_7$	$LaCr_2Al_{20}$	(Al)
6	99.58	0.03	0.39	$Al_{11}La_3$	$LaCr_2Al_{20}$	(Al)
7	99.45	0.11	0.44	$Al_{11}La_3$	$LaCr_2Al_{20}$	(Al)
8	99.34	0.23	0.43	$Al_{11}La_3$	$LaCr_2Al_{20}$	(Al)
9	99.20	0.35	0.45	$Al_{11}La_3$	$LaCr_2Al_{20}$	(Al)
10	99.15	0.46	0.39	$Al_{11}La_3$	$LaCr_2Al_{20}$	(Al)

Based on our results, we determined the phase equilibria at 600 °C in the Al-rich corner, see Figure 2. Since no data were available for the red dashed line, we took it from the ternary phase diagram drawn in the literature at 500 °C [81,82].

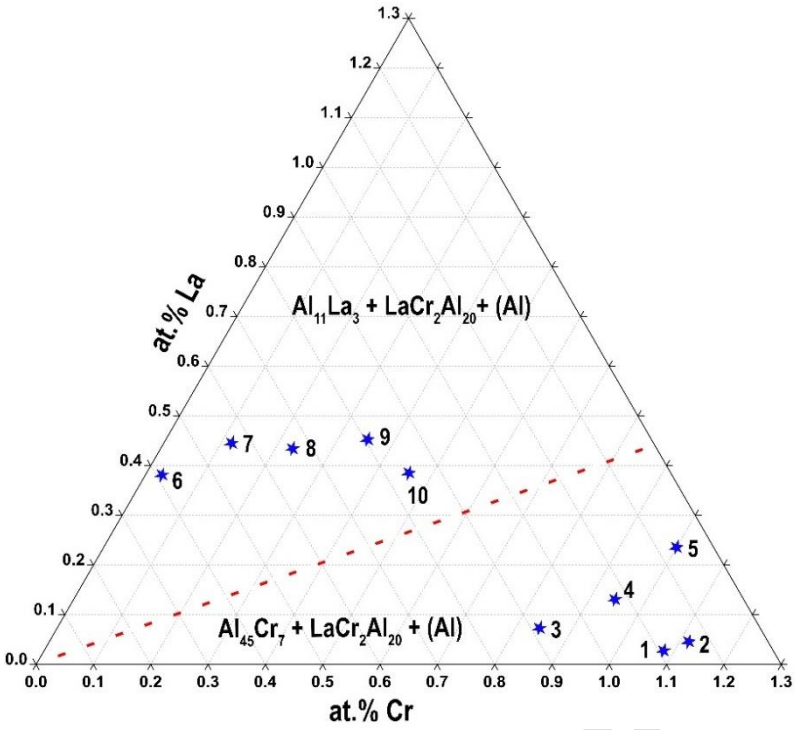

Figure 2. Isothermal section through the diagram of the ternary phase Al-Cr-La at 600 °C

3.1 DSC analysis

The DSC analysis was performed to determine the phase transformation temperatures. Based on the results, two different melting sequences can be recognized. For the samples with increased Cr content, we can recognize two peaks; the melting sequence for samples 1-5 is therefore as follows:

$$LaCr_2Al_{20} + (Al) + Al_{45}Cr_7 \leftrightarrow Al_{45}Cr_7 + L \leftrightarrow L \quad (1)$$

As an example, the representative part of the heating DSC curve of sample 3 is reported in Figure 3(a). We ascribe the low temperature large asymmetric peak to the melting of the ternary $LaCr_2Al_{20}$ phase and in the same peak the mixture $Al_{45}Cr_7$ + (Al) also melts. The second small peak (721±1 °C) belongs to the complete melting of the alloys.

The samples with increased La content (6-10) have three peaks; the melting sequence is as follows:

$$Al_{11}La_3 + (Al) + LaCr_2Al_{20} \leftrightarrow LaCr_2Al_{20} + Al_{45}Cr_7 + L \leftrightarrow Al_{45}Cr_7 + L \leftrightarrow L \quad (2)$$

The relevant part of the heating DSC curve of sample 10 is shown in Figure 3(b). In this case we were able to distinguish the lower temperature peaks: at 633±1 °C we have the melting of the mixture of $Al_{11}La_3$ + (Al) and at 645±1 °C the melting of the $LaCr_2Al_{20}$ ternary phase. The last peak at higher temperature (765±1 °C) fits the complete melting of the sample.

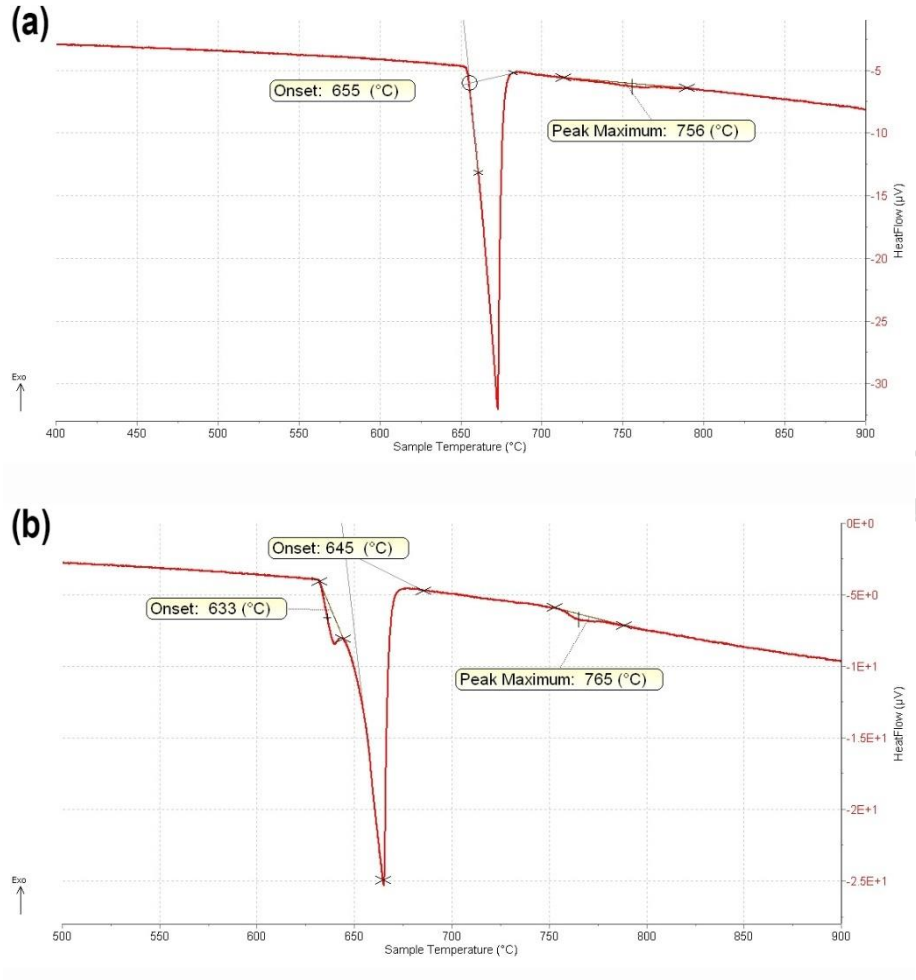

Figure 3. DSC heating curves of sample 3 (a) and sample 10 (b)

3.2 Metallography observations

The metallographic analysis of the annealed samples shows that the microstructure changes from that in Figure 4(a) (alloys 1–5, with higher Cr content) to that in Figure 4(b) (alloys 6–10, with higher La content). This difference can be clearly seen in Figure 4, in which sample 1 (samples with higher Cr content, Figure 4(a)) is compared with sample 8 (samples with higher La content, Figure 4(b)). The main microstructural difference lies in the binary phase formed: alloys with higher Cr have an $Al_{45}Cr_7$ phase (large grey phases in Figure 4(a)), while alloys with higher La content contain the $Al_{11}La_3$ phase (small white phases along the grain boundaries in Figure 4(b)), which is mixed with (Al). All alloys analysed also contain a (Al) phase and the ternary $LaCr_2Al_{20}$ phase (small white phases in Figure 4(a) and large grey phases in Figure 4(b)). In this section we present only the most representative results; the remaining ones can be found in the supplementary material.

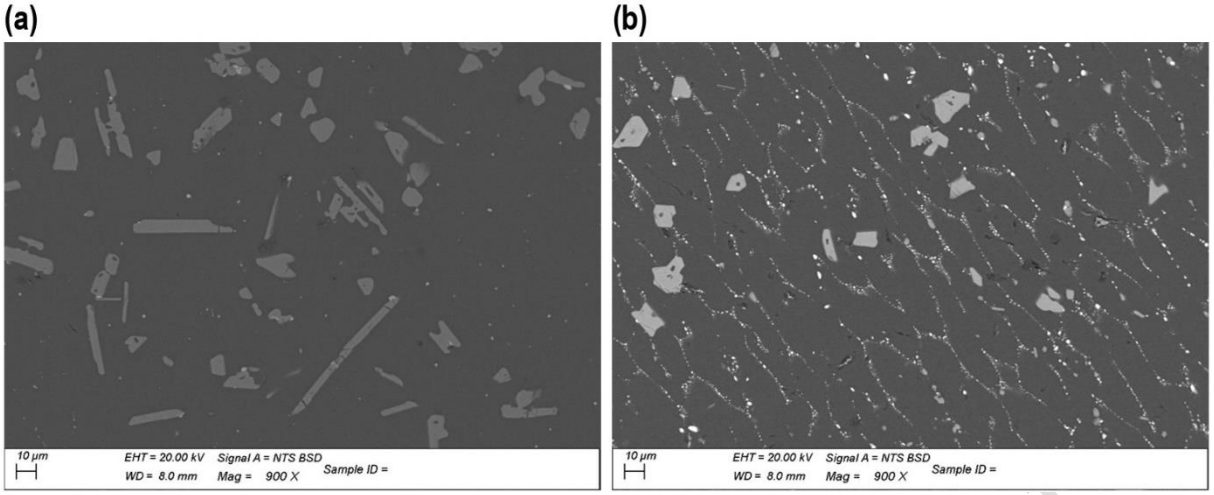

Figure 4. SEM-BSE images of the microstructure of sample 1 (a) and sample 8 (b)

To confirm the above estimates of the equilibrium phases, present in the samples (Table 4 and Figure 4), an EDXS analysis was performed. Figure 5 shows the EDXS analysis of sample 1 (Figure 5(a)) and sample 8 (Figure 5(b)). It is obvious that sample 1 (Figure 5(a)) consists of 3 phases, namely (Al), which is essentially the matrix, the binary phase $Al_{45}Cr_7$ (spectrum 1 and 2) and the ternary phase $LaCr_2Al_{20}$ (spectrum 3). On the other hand, sample 8 also consists of 3 phases, namely (Al), which is essentially the matrix, the binary phase $Al_{11}La_3$ (spectrum 1), which co-precipitate with (Al) and the ternary phase $LaCr_2Al_{20}$ (spectrum 2). One interesting thing that can be seen in Figure 5(a) is that the ternary phase $LaCr_2Al_{20}$ can be found around the $Al_{45}Cr_7$ phase.. The morphology of the $LaCr_2Al_{20}$ phase, which frequently appears around $Al_{45}Cr_7$ particles, suggests that the ternary phase forms through a transformation involving the binary precursor. In alloys with higher Cr content, the growth of $LaCr_2Al_{20}$ is constrained by the initial distribution of the $Al_{45}Cr_7$ phase, resulting in smaller ternary phase dimensions. Conversely, in alloys with lower Cr content, the smaller volume of the binary precursor is entirely consumed during the transformation, allowing the τ phase to develop a larger, less restricted morphology.

Regarding the solubility observed in the microstructures of the analysed samples, there was a trend, i.e. in the samples with higher Cr content (1-5) only Cr was dissolved in the matrix, while in the samples with higher La content (6-10) only a small amount of La was dissolved (see supplementary material for data).

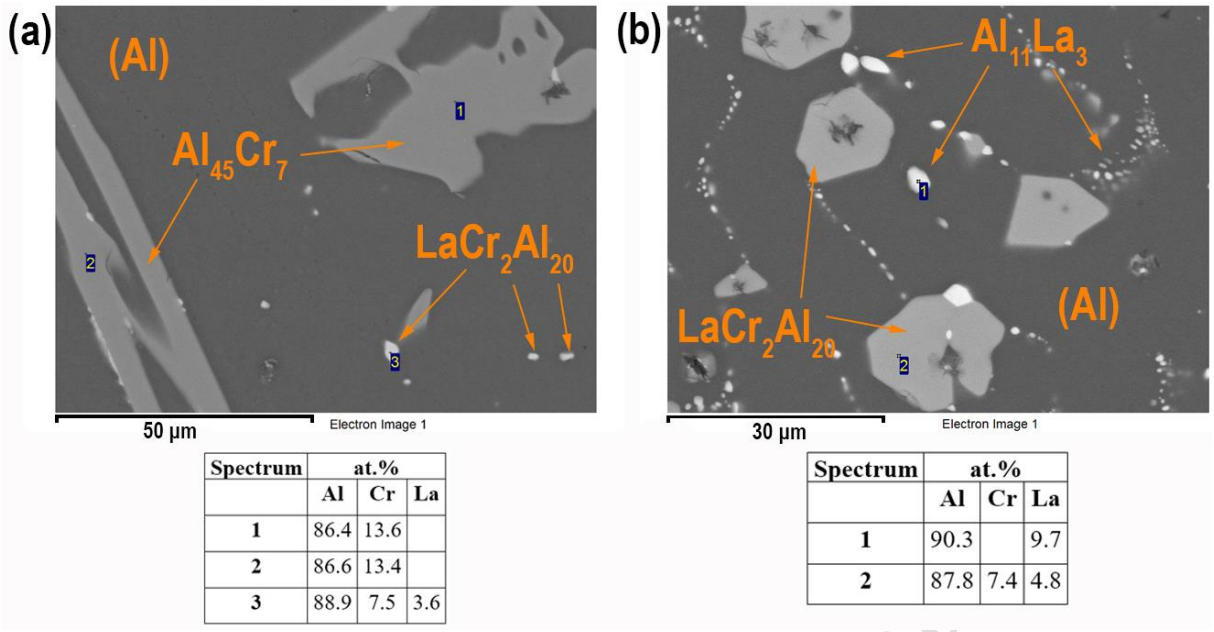

Spectrum	at.%		
	Al	Cr	La
1	86.4	13.6	
2	86.6	13.4	
3	88.9	7.5	3.6

Spectrum	at.%		
	Al	Cr	La
1	90.3		9.7
2	87.8	7.4	4.8

Figure 5. SEM-BSE images with EDXS analysis of sample 1 (a) and sample 8 (b), with the corresponding chemical composition of the phases

The observed microstructural differences, particularly the promotion of the τ phase by small La additions, are expected to affect the thermal stability and hardness of the alloys. From an industrial perspective, alloys with higher Cr content (alloys 1–5) appear more promising for the future development of Al-based materials, as they provide a balanced approach to improving properties while remaining economically viable.

4 Conclusions

Based on the results of this study, the following conclusions can be drawn:

- The equilibria at 600 °C involving the ternary $LaCr_2Al_{20}$ phase have been determined: in the alloys with higher Cr content (samples 1-5) together with $Al_{45}Cr_7$ phase and (Al) and, the alloys with higher La content (sample 6-10), consists of a $Al_{11}La_3$ + (Al). This is in agreement with the literature [80,81], even we do not have information about the composition neither the aspect of the microstructure of the samples.
- The study indicates that the ternary $LaCr_2Al_{20}$ (τ) phase forms immediately, even with a small (0.03 at.%) addition of La and/or Cr.
- The DSC investigation revealed the characteristic temperatures of Al-rich alloys, which can be used to plan the effective heat treatment of the potentially newly developed aluminium alloys.
- Since it was found that a small amount of La promotes the formation of the τ phase, positive effects on the future development of aluminium alloys are foreseeable from an economic point of view. From that point of view samples with higher Cr content seems to be more promising for the future development of aluminium-based materials.

Acknowledgments

We gratefully acknowledge the support of the work by the Slovenian Research And Innovation Agency (ARIS) program P1-0195 (B).

Authors contributions

Tilen Balaško: Conceptualization, Methodology, Investigation, Formal analysis, Writing & editing – original draft. Adam Zaky: Methodology, Investigation. Simona Delsante: Methodology, Formal analysis, Investigation, Writing - review & editing – original draft.

Data availability

The data supporting the results of this study are available upon reasonable request from the corresponding author, Tilen Balaško.

Conflicts of interest

The authors declare no conflict of interest

5 References

1. J.R. Davis, Alloying: Understanding the Basics, 1st ed., ASM International, Materials Park, OH, 2001, p.647.
2. S.D. Cramer, B.S. Covino Jr, ASM Handbook Volume 13B: Corrosion: Materials, ASM International, Materials Park, OH, 2005, p.704.
3. J.G. Kaufman, Introduction to Aluminium Alloys and Tempers, ASM International, Materials Park, OH, 2000, p.242.
4. E.L. Persson, Aluminum Alloys: Preparation, Properties and Applications, Nova Science Publishers, Incorporated, 2011, p.239.
5. G.E. Totten, M. Tiryakioğlu, O. Kessler, eds., Encyclopedia of aluminum and its alloys, CRC Press, Taylor & Francis Group, Boca Raton ; London ; New York, 2019, p.2892.
6. B. Stojanovic, M. Bukvic, I. Epler, Application of Aluminum and Aluminum Alloys in Engineering, Applied Engineering Letters, 3 (2) (2018) 52–62. https://doi.org/10.18485/aeletters.2018.3.2.2
7. M.-N. Su, B. Young, L. Gardner, The continuous strength method for the design of aluminium alloy structural elements, Engineering Structures, 122 (2016) 338–348. https://doi.org/10.1016/j.engstruct.2016.04.040
8. E. Georgantzia, M. Gkantou, G.S. Kamaris, Aluminium alloys as structural material: A review of research, Engineering Structures, 227 (2021) 111372. https://doi.org/10.1016/j.engstruct.2020.111372
9. D. Bhattacharjee, S. Chakrabarti, Future Landscape of Structural Materials in India, Springer Nature Singapore, Singapore, 2022, p.353.
10. W. Zhang, J. Xu, Advanced lightweight materials for Automobiles: A review, Materials & Design, 221 (2022) 110994. https://doi.org/10.1016/j.matdes.2022.110994
11. A.W. Orłowicz, M. Mróz, M. Tupaj, A. Trytek, Materials Used in the Automotive Industry, Archives of Foundry Engineering, 15 (2015) 75–78.

https://doi.org/10.1515/afe-2015-0042

12. J. Hirsch, Aluminium Alloys for Automotive Application, Materials Science Forum, 242 (1997) 33–50. https://doi.org/10.4028/www.scientific.net/MSF.242.33

13. T.P. Hovorun, K. V. Berladir, V.I. Pererva, S.G. Rudenko, A.I. Martynov, Modern materials for automotive industry, Journal of Engineering Sciences, 4 (2) (2017) f8–f18. https://doi.org/10.21272/jes.2017.4(2).f8

14. T. Trzepieciński, S.M. Najm, Current Trends in Metallic Materials for Body Panels and Structural Members Used in the Automotive Industry, Materials (Basel), 17 (3) (2024) 590. https://doi.org/10.3390/ma17030590

15. W. Miller, L. Zhuang, J. Bottema, A. Wittebrood, P. De Smet, A. Haszler, A. Vieregge, Recent development in aluminium alloys for the automotive industry, Materials Science and Engineering: A, 280 (1) (2000) 37–49. https://doi.org/10.1016/S0921-5093(99)00653-X

16. K. Sivanur, K. V. Umananda, D. Pai, Advanced materials used in automotive industry-a review, in: AIP Conference Proceedings, 2021: p.020032. https://doi.org/10.1063/5.0036149

17. A. Cascino, E. Meli, A. Rindi, A strategy for lightweight designing of a railway vehicle car body including composite material and dynamic structural optimization, Railway Engineering Science, 31 (2023) 340–350. https://doi.org/10.1007/s40534-023-00312-6

18. R. Soni, R. Verma, R. Kumar Garg, V. Sharma, A critical review of recent advances in the aerospace materials, Materials Today: Proceedings, 113 (2024) 180–184. https://doi.org/10.1016/j.matpr.2023.08.108

19. J. Singh, K. Srivastawa, S. Jana, C. Dixit, R. S, Advancements in Lightweight Materials for Aerospace Structures: A Comprehensive Review, Acceleron Aerospace Journal, 2 (3) (2024) 173–183. https://doi.org/10.61359/11.2106-2409

20. J.C. Williams, E.A. Starke, Progress in structural materials for aerospace systems, Acta Materialia, 51 (19) (2003) 5775–5799. https://doi.org/10.1016/j.actamat.2003.08.023

21. A. Ajanovic, R. Haas, The impact of energy policies in scenarios on GHG emission reduction in passenger car mobility in the EU-15, Renewable and Sustainable Energy Reviews, 68 (2017) 1088–1096. https://doi.org/10.1016/j.rser.2016.02.013

22. C. Lodi, A. Seitsonen, E. Paffumi, M. De Gennaro, T. Huld, S. Malfettani, Reducing CO 2 emissions of conventional fuel cars by vehicle photovoltaic roofs, Transportation Research Part D: Transport and Environment, 59 (2018) 313–324. https://doi.org/10.1016/j.trd.2018.01.020

23. G. Fontaras, P. Dilara, The evolution of European passenger car characteristics 2000-2010 and its effects on real-world CO2 emissions and CO2 reduction policy, Energy Policy, 49 (2012) 719–730. https://doi.org/10.1016/j.enpol.2012.07.021

24. Y. Kazancoglu, M. Ozbiltekin-Pala, Y.D. Ozkan-Ozen, Prediction and evaluation of greenhouse gas emissions for sustainable road transport within Europe, Sustainable Cities and Society, 70 (2021) 102924. https://doi.org/10.1016/j.scs.2021.102924

25. European Commission: Directorate-General for Mobility and Transport, EU transport in figures – Statistical pocketbook 2017, Publications Office, Luxembourg, 2017.

https://doi.org/10.2832/041248

26. T. Haas, H. Sander, Decarbonizing Transport in the European Union: Emission Performance Standards and the Perspectives for a European Green Deal, Sustainability, 12 (20) (2020) 8381. https://doi.org/10.3390/su12208381

27. S. Tsiakmakis, G. Fontaras, B. Ciuffo, Z. Samaras, A simulation-based methodology for quantifying European passenger car fleet CO2 emissions, Applied Energy, 199 (2017) 447–465. https://doi.org/10.1016/j.apenergy.2017.04.045

28. T. Hottle, C. Caffrey, J. McDonald, R. Dodder, Critical factors affecting life cycle assessments of material choice for vehicle mass reduction, Transportation Research Part D: Transport and Environment, 56 (2017) 241–257. https://doi.org/10.1016/j.trd.2017.08.010

29. Y. Xu, Z. Peng, D. Ding, W. Zhang, Y. Gao, G. Chen, Y. Xie, Y. Liao, Effect of La Addition on Microstructure and Properties of Al-0.2Fe-0.06Cu Alloy, Metals (Basel), 12 (2) (2022). https://doi.org/10.3390/met12020211

30. M. Hosseinifar, D. V. Malakhov, Effect of Ce and La on microstructure and properties of a 6xxx series type aluminum alloy, Journal of Materials Science, 43 (2008) 7157–7164. https://doi.org/10.1007/s10853-008-3022-2

31. H. Jiang, S. Li, L. Zhang, J. He, Q. Zheng, Y. Song, Y. Li, J. Zhao, The influence of rare earth element lanthanum on the microstructures and properties of as-cast 8176 (Al-0.5Fe) aluminum alloy, Journal of Alloys and Compounds, 859 (2021) 157804. https://doi.org/10.1016/j.jallcom.2020.157804

32. W.H. Yuan, B.L. An, Effect of la addition on the microstructures and mechanical properties of 7075 aluminum alloy, Advanced Materials Research, 152–153 (2011) 1810–1813. https://doi.org/10.4028/www.scientific.net/AMR.152-153.1810

33. Q. Li, T. Xia, Y. Lan, W. Zhao, L. Fan, P. Li, Effect of rare earth cerium addition on the microstructure and tensile properties of hypereutectic Al-20%Si alloy, Journal of Alloys and Compounds, 562 (2013) 25–32. https://doi.org/10.1016/j.jallcom.2013.02.016

34. A.E. Medvedev, M.Y. Murashkin, N.A. Enikeev, R.Z. Valiev, P.D. Hodgson, R. Lapovok, Enhancement of mechanical and electrical properties of Al-RE alloys by optimizing rare-earth concentration and thermo-mechanical treatment, Journal of Alloys and Compounds, 745 (2018) 696–704. https://doi.org/10.1016/j.jallcom.2018.02.247

35. R. Pérez-Bustamante, A. Reyna-Cruz, D.C. Acosta-Peña, C.R. Santillán-Rodríguez, J.A. Matutes-Aquino, F. Pérez-Bustamante, M.C. Maldonado-Orozco, J. Aguilar-Santillán, R. Martínez-Sánchez, Effect of cerium/lanthanum addition on microstructure and mechanical properties of Al7075 alloy via mechanical alloying and sintering, Journal of Rare Earths, 34 (4) (2016) 420–427. https://doi.org/10.1016/S1002-0721(16)60043-1

36. P. Tang, W. Li, Y. Zhao, K. Wang, W. Li, F. Zhan, Influence of strontium and lanthanum simultaneous addition on microstructure and mechanical properties of the secondary Al-Si-Cu-Fe alloy, Journal of Rare Earths, 35 (5) (2017) 485–493. https://doi.org/10.1016/S1002-0721(17)60938-4

37. E.A. De La Torre, R. Pérez-Bustamante, J. Camarillo-Cisneros, C.D. Gómez-Esparza, H.M. Medrano-Prieto, R. Martínez-Sánchez, Mechanical properties of the A356 aluminum alloy modified with La/Ce, Journal of Rare Earths, 31 (8) (2013) 811–816. https://doi.org/10.1016/S1002-0721(12)60363-9

38. T. Balaško, A. Nagode, J. Li, J. Medved, Microstructure evolution during solution annealing of an Al–Zn–Mg–Cu alloy with La additions, Scientific Reports, 15 (2025) 3845. https://doi.org/10.1038/s41598-025-88490-7

39. J.-O. Andersson, T. Helander, L. Höglund, P. Shi, B. Sundman, Thermo-Calc & DICTRA, computational tools for materials science, Calphad, 26 (2) (2002) 273–312. https://doi.org/10.1016/S0364-5916(02)00037-8

40. Thermo-Calc Software TCAL Al-base Alloy Database version 9, https://thermocalc.com/products/databases/aluminum-based-alloys/

41. J.L. Murray, The Al-Cr (aluminum-chromium) system, Journal of Phase Equilibria, 19 (1998) 367–375. https://doi.org/10.1007/BF02735058

42. W. Köster, E. Wachtel, K. Grube, Aufbau und magnetische Eigenschaften der Aluminium-Chrom-Legierungen, International Journal of Materials Research, 54 (7) (1963) 393–401. (in German) https://doi.org/10.1515/ijmr-1963-540702

43. H. Okamoto, Al-Cr (Aluminum-Chromium), Journal of Phase Equilibria and Diffusion, 29 (2008) 112–113. https://doi.org/10.1007/s11669-007-9225-4

44. G. Kurtuldu, P. Jessner, M. Rappaz, Peritectic reaction on the Al-rich side of Al–Cr system, Journal of Alloys and Compounds, 621 (2015) 283–286. https://doi.org/10.1016/j.jallcom.2014.09.174

45. J.G. Costa Neto, S. Gama, C.A. Ribeiro, Experimental study of the Al Cr equilibrium diagram, Journal of Alloys and Compounds, 182 (2) (1992) 271–280. https://doi.org/10.1016/0925-8388(92)90601-5

46. N. Saunders, V.G. Rivlin, Thermodynamic characterization of Al–Cr, Al–Zr, and Al–Cr–Zr alloy systems, Materials Science and Technology, 2 (6) (1986) 520–527. https://doi.org/10.1179/mst.1986.2.6.520

47. T. Ohnishi, Y. Nakatani, K. Okabayashi, Crystal Structures of Intermetallic θ, η and ε Phases in Al-Cr System, Bulletin of University of Osaka Prefecture. Series A, Engineering and natural sciences, 24 (2) (1976) 183–191. https://doi.org/10.24729/00008713

48. B. Grushko, B. Przepiórzyński, E. Kowalska-Strzęciwilk, M. Surowiec, New phase in the high-Al region of Al-Cr, Journal of Alloys and Compounds, 420 (1-2) (2006) L1–L4. https://doi.org/10.1016/j.jallcom.2005.10.046

49. F. Stein, C. He, I. Wossack, The liquidus surface of the Cr–Al–Nb system and re-investigation of the Cr–Nb and Al–Cr phase diagrams, Journal of Alloys and Compounds, 598 (2014) 253–265. https://doi.org/10.1016/j.jallcom.2014.02.045

50. B. Hu, W.-W. Zhang, Y. Peng, Y. Du, S. Liu, Y. Zhang, Thermodynamic reassessment of the Al–Cr–Si system with the refined description of the Al–Cr system, Thermochimica Acta, 561 (2013) 77–90. https://doi.org/10.1016/j.tca.2013.03.033

51. Y. Liang, C. Guo, C. Li, Z. Du, Thermodynamic modeling of the Al–Cr system,

Journal of Alloys and Compounds, 460 (1-2) (2008) 314–319. https://doi.org/10.1016/j.jallcom.2007.06.046

52. B. Grushko, B. Przepiórzyński, D. Pavlyuchkov, On the constitution of the high-Al region of the Al–Cr alloy system, Journal of Alloys and Compounds, 454 (1-2) (2008) 214–220. https://doi.org/10.1016/j.jallcom.2007.01.001

53. B. Grushko, E. Kowalska-Strzęciwilk, B. Przepiórzyński, M. Surowiec, Investigation of the Al–Cr γ-range, Journal of Alloys and Compounds, 402 (1-2) (2005) 98–104. https://doi.org/10.1016/j.jallcom.2005.04.144

54. K. Mahdouk, J.-C. Gachon, New Results about the Al-Cr Binary Phase Diagram, Archives of Metallurgy and Materials, (2001) 233–238. https://journals.pan.pl/dlibra/publication/151717/edition/132346/content

55. T. Helander, O. Tolochko, An experimental investigation of possible B2-ordering in the Al-Cr system, Journal of Phase Equilibria, 20 (1999) 57–60. https://doi.org/10.1361/105497199770335947

56. M. Audier, M. Durand-Charre, E. Laclau, H. Klein, Phase equilibria in the Al Cr system, Journal of Alloys and Compounds, 220 (1-2) (1995) 225–230. https://doi.org/10.1016/0925-8388(94)06010-X

57. S. Cui, I.-H. Jung, J. Kim, J. Xin, A coupled experimental and thermodynamic study of the Al-Cr and Al-Cr-Mg systems, Journal of Alloys and Compounds, 698 (2017) 1038–1057. https://doi.org/10.1016/j.jallcom.2016.12.298

58. M.J. Cooper, The structure of the intermetallic phase θ(Cr-Al), Acta Crystallographica, 13 (1960) 257–263. https://doi.org/10.1107/S0365110X60000571

59. K.A. Gschneidner, F.W. Calderwood, The Al−La (Aluminum-Lanthanum) system, Bulletin of Alloy Phase Diagrams, 9 (1988) 686–689. https://doi.org/10.1007/BF02883168

60. K.H.J. Buschow, THE LANTHANUM-ALUMINIUM SYSTEM, Philips Research Reports 20 (1965) 337–348. https://pearl-hifi.com/06_Lit_Archive/02_PEARL_Arch/Vol_16/Sec_53/Philips_Rsrch_Reports_1946_thru_1977/Philips%20Research%20Reports-20-1965.pdf

61. Z. Cao, G. Kong, C. Che, Y. Wang, and H. Peng, Experimental investigation of eutectic point in Al-rich Al-La, Al-Ce, Al-Pr and Al-Nd systems, Journal of Rare Earths, 35 (10) (2017) 1022–1028. https://doi.org/10.1016/S1002-0721(17)61008-1

62. Q. Yang, X. Liu, F. Bu, F. Meng, T. Zheng, D. Zhang, J. Meng, First-principles phase stability and elastic properties of Al–La binary system intermetallic compounds, Intermetallics, 60 (2015) 92–97. https://doi.org/10.1016/j.intermet.2015.02.007

63. J. Wang, Thermodynamic optimization for al-la system, Calphad, 18 (3) (1994) 269–272. https://doi.org/10.1016/0364-5916(94)90033-7

64. R.P. Elliott, F.A. Shunk, The Al−La (Aluminum-Lanthanum) system, Bulletin of Alloy Phase Diagrams, 2 (1981) 219–221. https://doi.org/10.1007/BF02881485

65. L. Jin, Y.-B. Kang, P. Chartrand, C.D. Fuerst, Thermodynamic evaluation and optimization of Al–La, Al–Ce, Al–Pr, Al–Nd and Al–Sm systems using the Modified Quasichemical Model for liquids, Calphad, 35 (1) (2011) 30–41.

https://doi.org/10.1016/j.calphad.2010.11.002

66. S.H. Zhou, R.E. Napolitano, Phase equilibria and thermodynamic limits for partitionless crystallization in the Al–La binary system, Acta Materialia, 54 (3) (2006) 831–840. https://doi.org/10.1016/j.actamat.2005.10.013

67. G. Borzone, N. Parodi, R. Ferro, J. Bros, J. Dubès, M. Gambino, Heat capacity and phase equilibria in rare earth alloy systems. R-rich R-Al alloys (R=La, Pr and Nd), Journal of Alloys and Compounds, 320 (2) (2001) 242–250. https://doi.org/10.1016/S0925-8388(00)01471-7

68. G. Cacciamani, R. Ferro, Thermodynamic modeling of some aluminium-rare earth binary systems: Al-La, Al-Ce and Al-Nd, Calphad. 25 (4) (2001) 583–597. https://doi.org/10.1016/S0364-5916(02)00009-3

69. F. Yin, X. Su, Z. Li, M. Huang, Y. Shi, A thermodynamic assessment of the La–Al system, Journal of Alloys and Compounds, 302 (1-2) (2000) 169–172. https://doi.org/10.1016/S0925-8388(00)00679-4

70. A. Juarez-Hernandez, H. Jones, Growth temperatures and microstructure selection during Bridgman solidification of hypereutectic Al–La and Al–Ce alloys, Journal of Crystal Growth, 208 (1-4) (2000) 442–448. https://doi.org/10.1016/S0022-0248(99)00400-5

71. A. Hawksworth, W.M. Rainforth, H. Jones, Solidification microstructure selection in the Al-rich Al–La, Al–Ce and Al–Nd systems, Journal of Crystal Growth, 197 (1-2) (1999) 286–296. https://doi.org/10.1016/S0022-0248(98)00955-5

72. G. Borzone, A.M. Cardinale, N. Parodi, G. Cacciamani, Aluminium compounds of the rare earths: enthalpies of formation of Yb-Al and La-Al alloys, Journal of Alloys and Compounds, 247 (1-2) (1997) 141–147. https://doi.org/10.1016/S0925-8388(96)02605-9

73. T.B. Massalski, H. Okamoto, P.R. Subramanian, L. Kacprzak, Binary Alloy Phase Diagrams, ASM International, Materials Park, OH, 1990, p. 287–1288.

74. O.M. Barabash, Yu.N. Kobal, Кристаллическая структура металлов и сплавов (Crystal Structures of Metals and Alloys), Naukova Dumka, Kiev, 1986. (in Russian)

75. E.M. Savitskii, V.F. Terekhova, A.V. Kholopov, Диаграмма состояния сплавов системы хром–лантан (Phase Diagram for Alloys in the Chromium-Lanthanum System), Russian Journal of Inorganic Chemistry, 5 (1960) 362–363. (in Russian)

76. V.M. Svechnikov, G.F. Kobzenko, M.V. Kireev, V.G. Ivanchenko, Розчинність ітрію і лантану в хромі (Solubility of Yttrium and Lanthanum in Chromium), Dopovidi Akademiï nauk Ukraïn'skoï RSR, (1973) 167–170. (in Ukrainian)

77. S. Ray, J.P. Neumann, Calculation of the binary chromiun-lanthanide phase diagrams, Journal of Phase Equilibria, 17 (1996) 179–185. https://doi.org/10.1007/BF02648486

78. W. Chan, M.C. Gao, Ö.N. Doğan, P. King, A.D. Rollett, Thermodynamic Assessment of Cr-Rare Earth Systems, Journal of Phase Equilibria and Diffusion, 30 (2009) 578–586. https://doi.org/10.1007/s11669-009-9581-3

79. H. Okamoto, Supplemental Literature Review of Binary Phase Diagrams: Bi-Ga, Bi-Y, Ca-H, Cd-Fe, Cd-Mn, Cr-La, Ge-Ru, H-Li, Mn-Sr, Ni-Sr, Sm-Sn, and Sr-Ti, Journal of

Phase Equilibria and Diffusion, 36 (2015) 292–303. https://doi.org/10.1007/s11669-015-0370-x

80. P.I. Kripyakevich, O.S. Zarechnyuk, Сполуки RCr2Al20 в системах рідкісноземельних елементів і Ca та їх кристалічна структура (The Compounds RCr2Al20 in the Rare Earth and Ca Systems and Their Crystal Structure), Dopovidi Akademiï nauk Ukraïn'skoï RSR, 4 (1968) 364–367. (in Ukrainian)

81. O.J. Emes-Misenko, Дослідження фазових рівноваг у системах лантан–хром–алюміній та лантан–марганець–алюміній в ділянці з низьким вмістом лантану (Investigation of the phase equilibria in the lanthanum-chromium-aluminum and lanthanum-manganese-aluminum systems in the region of low lanthanum content), Visnyk of the Lviv University. Series Chemistry, 12 (1971) 12–14. (in Ukrainian)

82. L. Guzei and M. Materials Science International Team, Al-Cr-La Ternary Phase Diagram Evaluation · Phase diagrams, crystallographic and thermodynamic data: Datasheet from MSI Eureka in SpringerMaterials (https://materials.springer.com/msi/docs/sm_msi_r_10_019188_01), MSI Materials Science International Services GmbH, https://materials.springer.com/msi/docs/sm_msi_r_10_019188_01.

83. K.H.J. Buschow, J.H.N. Van Vucht, W.W. Van Den Hoogenhof, Note on the crystal structure of the ternary rare earth-3d transition metal compounds of the type RT4Al8, Journal of the Less Common Metals, 50 (1) (1976) 145–150. https://doi.org/10.1016/0022-5088(76)90261-7

84. L.J. Treadwell, J.D. McAlpin, D.C. Schmitt, M.J. Kangas, M.T. Sougrati, N. Haldolaarachchige, D.P. Young, J.C. Jumas, J.Y. Chan, Investigation of Fe incorporation in LnCr2Al20 (Ln = La, Gd, Yb) with 57Fe Mössbauer and single crystal X-ray diffraction, Inorganic Chemistry, 52 (9) (2013) 5055–5062. https://doi.org/10.1021/ic302805n

85. R. Pöttgen, O. Janka, CeCr2Al20 -type intermetallics – structure-property relationships, Reviews in Inorganic Chemistry, 43 (3) (2023) 357–383. https://doi.org/10.1515/revic-2023-0012

86. W.J. Boettinger, U.R. Kattner, K.-W. Moon, J.H. Perepezko, DTA and heat-flux DSC measurements of alloy melting and freezing, in: J.-C. Zhao (E.), Methods for Phase Diagram Determination, 1st ed., Elsevier, 2007, p.151–221. https://doi.org/10.1016/B978-0-08-044629-5.X5000-9

List of figures captions

Figure 6. Isothermal section through the ternary phase diagram of Al-Cr-La at 500 °C [82]

Figure 7. Isothermal section through the diagram of the ternary phase Al-Cr-La at 600 °C

Figure 8. DSC heating curves of sample 3 (a) and sample 10 (b)

Figure 9. SEM-BSE images of the microstructure of sample 1 (a) and sample 8 (b)

Figure 10. SEM-BSE images with EDXS analysis of sample 1 (a) and sample 8 (b), with the corresponding chemical composition of the phases

List of table captions

Table 5. Al-Cr crystal structure data

Table 6. Al-La crystal structure data

Table 7. Al-Cr-La crystal structure data

Table 8. Chemical composition of the samples with the corresponding equilibrium phases in the microstructure